






MR Elastography for Classification of Focal Liver Lesions Using Viscoelastic Parameters: A Pilot Study Based on Intrinsic and Extrinsic Activations

Amirhosein Baradaran Najar, MSc,^{1,2}  Guillaume Gilbert, PhD,^{3,4}  Elige Karam, MD,^{2,4} Anton Volniansky, MD,⁴  Audrey Fohlen, MD, PhD,⁴ Maxime Barat, MD, PhD,^{2,4}  Emmanuel Montagnon, PhD,² Hélène Castel, MD,⁵ Jeanne-Marie Giard, MD, MPH,⁵ Bich N. Nguyen, MD,⁶ Guy Cloutier, PhD, Eng,^{2,4,7,8} An Tang, MD, MSc,^{2,4*}  and Elijah Van Houten, PhD, Eng^{1,9}

Background: Intrinsic activation MR elastography (iMRE) uses cardiovascular pulsations to assess tissue viscoelastic properties. Applying it to focal liver lesions extends its capabilities.

Purpose: To assess the viscoelastic parameters of focal liver lesions measured by iMRE and compare its diagnostic performance with extrinsic MRE (eMRE) for differentiating malignant and benign lesions.

Study type: Prospective.

Population: A total of 55 participants underwent MRI with research MRE sequences; 32 participants with 17 malignant and 15 benign lesions underwent both iMRE and eMRE.

Field Strength/Sequence: iMRE at ~1 Hz heart rate used a 3 T scanner with a modified four-dimensional (4D)-quantitative flow gradient-echo phase contrast and low-velocity encoding cardiac-triggered technique. eMRE employed a gradient-echo sequence at 30, 40, and 60 Hz.

Assessment: Liver displacements were measured using 4D-phase contrast and reconstructed via a nonlinear inversion algorithm to determine shear stiffness (SS) and damping ratio (DR). iMRE parameters were normalized to the corresponding values from the spleen. Lesions were manually segmented, and image quality was reviewed.

Statistical Tests: Kruskal–Wallis, Mann–Whitney, Dunn’s test, and areas under receiver operating characteristic curves (AUC) were assessed.

Results: SS was significantly higher in malignant than benign lesions with iMRE at 1 Hz (3.69 ± 1.31 vs. 1.63 ± 0.45) and eMRE at 30 Hz (3.76 ± 1.12 vs. 2.60 ± 1.26 kPa), 40 Hz (3.76 ± 1.12 vs. 2.60 ± 1.26 kPa), and 60 Hz (7.32 ± 2.87 vs. 2.48 ± 1.12 kPa). DR was also significantly higher in malignant than benign lesions at 40 Hz (0.36 ± 0.11 vs. 0.21 ± 0.01) and 60 Hz (0.89 ± 0.86 vs. 0.22 ± 0.09). The AUC were 0.86 for iMRE SS, 0.87–0.98 for eMRE SS, 0.47 for iMRE DR, and 0.62–0.86 for eMRE DR.

View this article online at [wileyonlinelibrary.com](https://onlinelibrary.wiley.com/doi/10.1002/jmri.29633). DOI: 10.1002/jmri.29633

Received May 31, 2024, Accepted for publication Oct 6, 2024.

*Address reprint requests to: An Tang, Department of Radiology, Radiation Oncology and Nuclear Medicine, Université de Montréal, 1000, rue Saint-Denis, D03.5431, Quebec, Canada H2X 0C1. E-mail: an.tang@umontreal.ca
Guy Cloutier, An Tang, and Elijah Van Houten share co-senior authorships.

From the ¹Département de Génie Mécanique, Université de Sherbrooke, Sherbrooke, Quebec, Canada; ²Laboratoire clinique de traitement de l’image (LCTI), Centre de recherche du Centre hospitalier de l’Université de Montréal (CRCHUM), Montreal, Quebec, Canada; ³MR Clinical Science, Philips Healthcare, Mississauga, Ontario, Canada; ⁴Department of Radiology, Radiation Oncology and Nuclear Medicine, Université de Montréal, Montreal, Quebec, Canada; ⁵Department of Hepatology and Liver Transplantation, Centre Hospitalier de l’Université de Montréal (CHUM), Montreal, Quebec, Canada; ⁶Service of Pathology, Centre hospitalier de l’Université de Montréal (CHUM), Montreal, Quebec, Canada; ⁷Institute of Biomedical Engineering, Université de Montréal, Montreal, Quebec, Canada; ⁸Laboratory of Biorheology and Medical Ultrasonics (LBUM), Centre de recherche du Centre hospitalier de l’Université de Montréal (CRCHUM), Montreal, Quebec, Canada; and ⁹Centre de recherche du Centre hospitalier de l’Université de Sherbrooke (CRCHUS), Sherbrooke, Quebec, Canada

Additional supporting information may be found in the online version of this article

This is an open access article under the terms of the [Creative Commons Attribution-NonCommercial-NoDerivs](https://creativecommons.org/licenses/by-nc-nd/4.0/) License, which permits use and distribution in any medium, provided the original work is properly cited, the use is non-commercial and no modifications or adaptations are made.

Data Conclusion: Cardiac-activated iMRE can characterize liver lesions and differentiate malignant from benign lesions through normalized SS maps.

Level of Evidence: 2

Technical Efficacy: Stage 2

J. MAGN. RESON. IMAGING 2025;61:2525–2540.

The assessment of liver mechanical properties through magnetic resonance elastography (MRE) plays a role in understanding liver health and the effectiveness of treatments.^{1–3} Prior work indicates that a mere 1-kPa increase in liver stiffness corresponds to a 4% increase in the likelihood of hepatocellular carcinoma (HCC),² along with a 16.3% rise in the risk of tumor recurrence after resection. Consequently, mechanical properties can serve as biomarkers to grade the progression of liver cancer.⁴

MRE can be used to generate viscoelastic mechanical property images across various frequencies.⁵ Traditionally, MRE measurements involve inducing mechanical waves through external vibration sources at frequencies typically between 30 and 100 Hz.^{6–8} However, in some organs such as the brain and liver, intrinsic MRE (iMRE) may capitalize on physiological tissue motion induced by cardiovascular pulsations, thus eliminating the need for external vibration sources.^{9–11} iMRE offers several advantages over extrinsic MRE. Most notably, it removes the requirement for external vibration sources and the need for additional hardware, thus broadening the number of scanners on which it could be implemented. Moreover, iMRE can solve the problem of poor shear wave penetration.⁹ Additionally, iMRE measurements occur at physiological frequencies, aligning better with the biomechanical characteristics of living tissues.⁹ This is important as tissue mechanical properties can exhibit considerable frequency dependencies. Using physiological frequencies allows us to study tissue mechanical properties under conditions that closely mimic natural physiological states, which are important for understanding how these properties affect tissue function and health.¹²

In liver tumor characterization, parameters such as the complex shear modulus representing stiffness ($|G^*|$), the storage modulus (real part of G^*), the loss modulus (imaginary part of G^*), and the shear wave speed (c), phase angle (φ) of the complex modulus have been employed.^{6–8,13} The damping ratio (DR), defined as the ratio of loss modulus to storage modulus, has been primarily associated with the characterization of steatohepatitis, inflammation, and fibrosis.^{14–17} A proof-of-concept study using iMRE in the liver showed that storage modulus increased by 200% and DR decreased by 50% in a focal nodular hyperplasia relative to healthy liver.¹¹ However, iMRE has not been used to calculate viscoelastic parameters for characterizing and classifying a range of focal liver lesions.

This pilot study aimed to assess the viscoelastic parameters of focal liver lesions measured by nonlinear inversion

(NLI) iMRE and to compare the diagnostic performance of iMRE with eMRE for differentiating benign and malignant liver lesions.

Materials and Methods

Study Design

This prospective single-center study was conducted from March 2021 to April 2022 and received approval from the institutional review board. Informed written consent was obtained from all participants enrolled in this study.

Participant Selection

Participants were eligible if they: 1) were enrolled in a HCC surveillance program for chronic liver disease or cirrhosis; 2) underwent diagnostic MRI for characterization of a focal liver nodule; or 3) had a liver nodule ≥ 10 mm incidentally found at ultrasound, computed tomography (CT), or MRI that required further characterization. Participants were included in this pilot cohort if nodules were visible on MRI (reported by A.T., 18 years of experience in liver MRI). Participants were excluded if they: 1) had a contraindication to MRI (ie, insurmountable claustrophobia or pacemaker); 2) had chronic kidney disease preventing injection of gadolinium-based contrast agent; 3) had previously treated liver lesions; and 4) had no visible focal liver lesion on MRI.

Posteriori exclusion criteria were based on the absence of acceptable MRI image quality, incomplete multiparametric MRI scans, lesions smaller than 10 mm, inadequate image quality for segmentation purposes, and improper visibility of the spleen in the images assessed by three independent observers (A.T. and M.B., fellowship-trained abdominal radiologists with 1 year of experience; and E.K., fellowship-trained abdominal radiologist with 1 year of experience).

Index Tests

MRI examinations were performed on a 3 T scanner (Achieva TX, Philips Healthcare, Best, The Netherlands) using the integrated dual-channel body coil for transmission and a 16-channel body array for signal reception. All included participants underwent clinical contrast-enhanced MRI sequences, research iMRE, and research eMRE sequences.

Table 1 provides sequence parameters for iMRE, eMRE, and segmentation.

Intrinsic MRE was performed in the axial plane using a modified quantitative four-dimensional (4D) sequence consisting of a low-velocity encoding (VENC) cardiac-triggered phase-contrast sequence with three-dimensional (3D) motion-encoding across multiple time points within the cardiac cycle.¹⁸

Extrinsic MRE (30, 40, and 60 Hz) was performed using the eXpresso sequence¹⁹ with 3D motion-encoding and a commercially

Table 1. Acquisition Parameters for the Intrinsic, Segmentation, and Extrinsic MRE Sequences

Intrinsic			
Sequence	4D-Phase Contrast		
Number of slices	8		
Cardiac phases	8		
Echo time (msec)	9.2		
Field-of-view (mm ²)	320 × 320		
Spatial resolution (mm)	4 (isotropic)		
Breathing	breath-hold		
Repetition time (msec)	12.2		
Acceleration factor	2 (SENSE), 7 (EPI)		
VENC (cm/second)	5 in AP and RL, 10 in FH		
Scanning time (seconds)	14–22		
Extrinsic			
Sequence	Expresso		
Motion-encoding frequency	30 Hz	40 Hz	60 Hz
Field-of-view (mm ²)	320 × 320		
Spatial resolution (mm)	4 × 4		
Parallel imaging acceleration (SENSE)	1.5		
Slice thickness (mm)	4		
Number of breath-holds	4		
Motion-encoding gradient amplitude (mT/m)	19.6		
Flip angle (°)	20		
TE (msec)	6.9		
TR (msec)	108	81	71
Number of slices	9	9	8
Breath-hold duration (seconds)	16.7	12.5	10.9
eXpresso factor	3	3	2
Scanning time (seconds)	66.8	50	43.6
Segmentation			
Sequence	Balanced steady-state free-precession (bSSFP)		
Echo time (msec)	0.91		
Field-of-view (mm ²)	320 × 320		

Table 1. Continued

Segmentation	
Sequence	Balanced steady-state free-precession (bSSFP)
Spatial resolution (mm)	4 (isotropic)
Repetition time (msec)	1.83
Flip angle (degrees)	45°
Sequence	4D-Flow
VENC (cm/second)	110 in AP, RL, and FH
Other parameters	Same as the imaging sequence
VENC = velocity encoding; SENSE = sensitivity encoding; TE = echo time; TR = repetition time.	

available active transducer (Resoundant, Rochester, MN, USA). That sequence is a rapid multi-slice gradient-recalled echo MRE sequence leveraging fractional-encoding.

Two additional sequences were performed with the same geometry as for the intrinsic MRE sequence to allow for identification and segmentation of the large vessels present in the liver (arteries and veins). First, a balanced steady-state free-precession (bSSFP) sequence was performed as it provides a high signal for all fluid-containing regions. Second, a 4D-flow sequence was also performed to identify specifically arteries and veins that display high-velocity blood flow. That sequence was performed with exactly the same parameters as for the intrinsic MRE sequence but using a higher VENC of 110 cm/second in all three spatial directions.

In this study, all MRE sequences were conducted under breath-hold to mitigate respiratory motion, which is generally effective given participants' ability to perform consistent breath-holding. For the eXpresso sequence specifically, despite using four separate breath-holds to account for motion in different encoding directions, residual motion between breath-holds may still occur. The nonrigid registration has not been employed between breath-holds in eXpresso sequences as routinely practiced in other imaging modalities like intravoxel incoherent motion and dynamic contrast-enhanced due to concerns about potential phase information alteration in MRE applications.¹⁹

Nonlinear Inversion MR Elastography

Mechanical properties were derived from the measured displacements using a NLI algorithm.²⁰ The NLI algorithm iteratively updates a discretized description of the property distribution in a heterogeneous finite element model by minimizing differences between model displacements and motion measurements. In this study, viscoelastic governing equations were used as the model, similar to the approach by Gordon-Wylie et al.¹⁸ From this model, the complex shear modulus was calculated.

The complex shear modulus comprises the storage modulus (G'), the loss modulus (G''), and their magnitude ($|G^*|$). In this study, two parameters are presented: shear stiffness (SS) and DR. These parameters are formulated as follows:

$$SS = \frac{2^* |G^*|^2}{G' + |G^*|} \quad (1)$$

$$DR = \frac{G''}{2^* G'} \quad (2)$$

While NLI-MRE has been shown to be highly repeatable and precise for in vivo brain applications,²¹ this work presents the first application of NLI-MRE to the intrinsically and extrinsically excited liver. Here, we have employed the same NLI approach, which typically requires 2–3 hours, to analyze MRE liver data. SS and DR have been reported at all selected frequencies. The only difference between intrinsic and extrinsic cases is that, in the intrinsic case, the values for SS and DR were normalized to the corresponding values from the spleen. At low frequencies (~ 1 Hz), the shear modulus can only be determined relative to a nonunique scalar multiplier.¹² In this case, material properties are relative, so liver parameters are normalized by the mean values of the spleen, as a reference, to allow for comparability within the liver and lesion. Normalization was performed by separately calculating and normalizing SS and DR values given the reconstructed complex shear modulus values found in both organs. Although the DR is inherently a normalized parameter, we applied this additional normalization step using the spleen as a reference organ to ensure consistency with the reported SS values, such that all reported iMRE values are relative to the values observed in the spleen.

A spatial filter was applied during the reconstruction process to reduce noise and improve the smoothness of the mechanical maps. Specifically, a spatial frequency Gaussian filter, smaller than half the voxel size, was used to achieve this smoothing.

Image Analysis

For the segmentation, a radiologist (M.B.) performed manual delineation of the liver based on the bSSFP and 4D flow sequences for the entire cohort. The radiologist used clinical MR images to identify the lesion location. The identification of focal liver lesions was based on established criteria, including lesion size equal or greater than 10 mm, distinct morphological, signal, or enhancement differences compared to the background liver. The radiologist utilized 3D slicer²² to delineate the regions of interest (ROIs) on the MRE images. A sample ROI illustration has been included in Fig. S1 in the Supplemental Material.

The initial reconstruction results showed artifacts in the vessels for intrinsic analysis confirmed by three observers (A.T., M.B., and E.K.). Motion measurements within voxels containing a substantial portion of rapidly flowing blood can readily lead to motion estimates with aliasing issues, primarily due to the heightened motion sensitivity necessary for detecting small tissue velocities⁹; therefore, another radiologist (E.K.) segmented the vessels and spleen. These segmentations were used to allow the normalization of the liver mechanical parameters by the mean value of the same parameters within the spleen. To ensure the accuracy and reproducibility of ROI

identification, the second radiologist independently reviewed all segmentations and revised some of them. The same ROIs drawn for iMRE were duplicated for eMRE to ensure consistency in the measurement of viscoelastic parameters across both imaging modalities.

Reference Standard

The ground truth for liver lesion diagnosis was a composite reference standard that included contrast-enhanced MRI using Gd-BOPTA, or histopathology. Categorization and diagnosis of liver nodules were established according to LI-RADS reporting standards version 2018²³ by four radiologists (A.T., M.B., E.K., and A.F., abdominal radiologist, 16 years of experience) who were unaware of the findings of the research MRI studies.²³ Portal hypertension (determined by the presence of splenomegaly, ascites, or varices) and other conditions that may affect the mechanical properties of the spleen by increasing the portal venous pressure such as tumor invasion or bland thrombus in the portal vein, and mesenteric vein involvement were assessed based on MRI images by a radiologist (A.F.).

When available, histopathological evaluation performed according to the clinical standard of care was included to resolve cases when imaging results were inconclusive or indicative of malignancies other than HCC. Liver biopsy using 18-gauge core needles, surgical resection specimens, or liver explants was employed to obtain pathological diagnoses.

Interobserver Assessment

To evaluate interobserver agreement, a second radiologist (E.K.) independently performed repeated segmentations on 15 participants, and iMRE measurements were performed for this group. The SS and DR calculated from these segmentations were then assessed using the intraclass correlation coefficient (ICC).

Statistical Analysis

Statistical analyses were conducted using R (version 3.4.3; R Foundation) with the “lme4,” “pROC,” and “ggplot2” packages. A significance level of $P < 0.05$ was adopted, and 95% confidence intervals were calculated by bootstrapping using the “boot” package. Mean and standard deviation values were computed for lesions and background liver. Kruskal–Wallis tests were performed to compare multiple groups of lesions and gave a P -value that indicates whether there are statistically significant differences between the groups overall. The Dunn’s post hoc test performs pairwise comparisons between groups with larger populations to determine which specific groups differ, applying Bonferroni correction to adjust P -values (0.001). The Mann–Whitney U test was used to compare viscoelastic properties between liver lesions grouped as benign (including hemangioma, focal nodular hyperplasia, adenoma, LR-2, and LR-3) or malignant (LR-4, LR-5, metastasis, HCC, and cholangiocarcinoma). Sensitivity, specificity, positive predictive value, negative predictive value, and the area under the receiver operating characteristic curve (AUC) were computed for the participants who completed both iMRE and eMRE exams to allow head-to-head comparison of the diagnostic performance of these two methods. The cut-off for diagnostic performance was determined using the Youden Index, to provide the best balance between the sensitivity and specificity. AUCs were compared using the DeLong method.²⁴

Results

Participant and Observation Characteristics

Fifty-five participants (mean age: 60 ± 14 years [range 26–82], 34 male) were examined using MRE. Thirty-three underwent iMRE, 45 eMRE, and 32 both iMRE and eMRE. Figure 1 shows the flowchart of participant recruitment, including exclusions and technical failures of intrinsic and extrinsic MRE. A total of 22 participants were excluded from iMRE, of which 12 out of 55 (22%) were excluded due to the spleen not being visible. For eMRE, 10 participants were excluded. The intrinsic MRE cohort included 16 benign and

17 malignant lesions and the extrinsic MRE cohort included 23 benign and 22 malignant lesions. Table 2 summarizes characteristics of participants and lesions included in the study. Diseases which may affect the normalized SS by increasing spleen stiffness was present in 31% (17/55) of participants. Portal hypertension was observed in 15% (5/33) of participants who underwent iMRE.

The acquisition time for iMRE varied between 14 and 22 seconds (one breath-hold), depending on the subject's heart rate. For eMRE, the total acquisition time at 30 Hz was 4 breath-holds of 16.7 seconds each, totaling 66.8 seconds; at

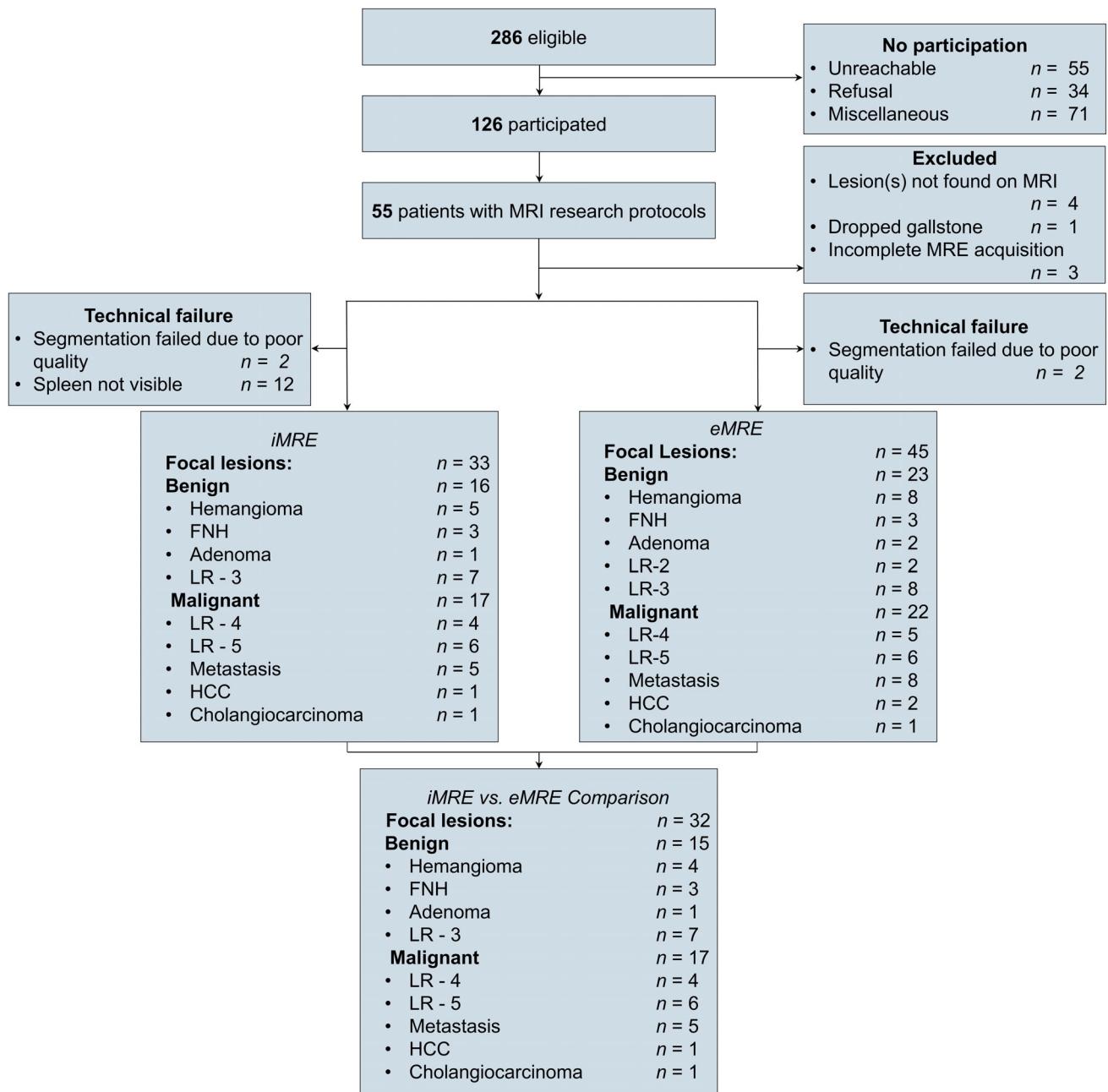


Figure 1: Flowchart of participant selection. LR indicates the category levels within Liver Imaging Reporting and Data System (LI-RADS). FNH = focal nodular hyperplasia; HCC = pathology-proven hepatocellular carcinoma.

Table 2. Characteristics of the Study Participants

Characteristics	Values
Sex	
Male	34
Female	21
Age (years)	
Mean \pm SD (range)	60 \pm 14 (26–82)
BMI (kg/m ²)	27 \pm 5 (18–41)
<25	17 (30.9)
\geq 25 and <30	22 (40.1)
\geq 30 and <40	15 (27.3)
\geq 40	1 (1.8)
Ethnic category	
Arab	3 (5.4)
Asian	4 (7.3)
Black	1 (1.8)
Caucasian	43 (78.2)
Hispanic	3 (5.4)
Indian	1 (1.8)
Conditions that may affect the mechanical properties of the spleen	
Portal hypertension	13 (23.6)
Tumor in a vein	1 (1.8)
Bland thrombus in the portal vein	2 (3.6)
Mesenteric vein involvement	1 (1.8)
Focal liver lesion	55
Hemangioma	10 (18.2)
Focal nodular hyperplasia	3 (5.4)
Hepatocellular adenoma	2 (3.6)
Cholelithiasis	1 (1.8)
LR-2	2 (3.6)
LR-3	9 (16.4)
LR-4	6 (11.1)
LR-5	6 (11.1)
Metastasis	11 (20.0)
HCC	4 (7.3)
Cholangiocarcinoma	1 (1.8)
Size of focal liver lesions	
Hemangioma	25.6 \pm 18.7

Table 2. Continued

Characteristics	Values
Focal nodular hyperplasia	17.0 ± 4.2
Hepatocellular adenoma	27.5 ± 20.5
LR-2	12.8 ± 7.6
LR-3	17.3 ± 5.6
LR-4	17.8 ± 4.2
LR-5	23.6 ± 7.4
Metastasis	29.2 ± 19.4
HCC	10.0 ± 7.1
Cholangiocarcinoma	35
Heart rate (beats per minute)	70 ± 11 (46–91)

Values are mean \pm SD (range) or number (percentage).

BMI = body mass index; HCC = hepatocellular carcinoma; SD = standard deviation.

40 Hz, it was 4 breath-holds of 12.5 seconds each, totaling 50 seconds; and at 60 Hz, it was 4 breath-holds of 10.9 seconds each, totaling 43.6 seconds. In addition to these times, there was a default inter-breath-hold period of 10 seconds, which could be adjusted based on the subject's needs. Including these intervals, the total acquisition time for eMRE was approximately 280 seconds.

Mechanical Parameters Measurements

Figure 2 shows representative images of a cholangiocarcinoma including color parametric maps of iMRE and eMRE for SS

and DR. In the iMRE color maps for SS and DR, the iMRE map of normalized SS shows an increase in stiffness within the lesion area. This increase is also observed in the SS and DR maps generated from eMRE. Figure 3 shows representative images of normalized SS by iMRE and SS by eMRE in four cases of benign and malignant liver lesions. Both the normalized SS from iMRE and SS from eMRE demonstrate increased stiffness in the area surrounding different types of lesions. The mechanical maps in these figures appear very smooth due to the application of a spatial filter. There are some blank regions in the maps of mechanical parameters,

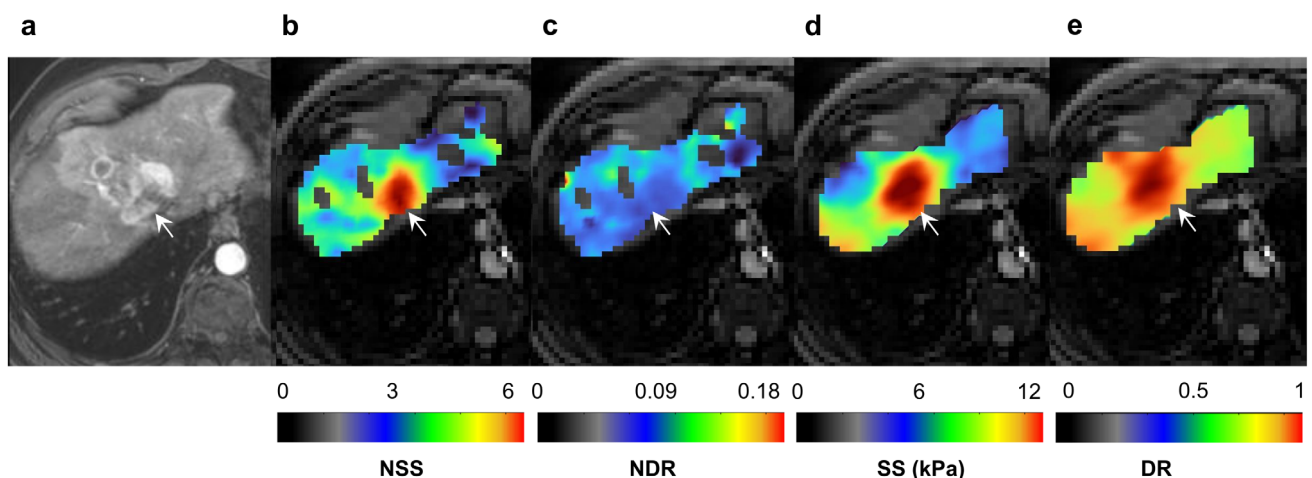


Figure 2: A 79-year-old man with a cholangiocarcinoma. (a) Arterial phase imaging. (b) Intrinsic MR elastography (iMRE) reconstruction of normalized SS (normalized to the mean of shear stiffness in the spleen) reveals elevated stiffness in the tumor area. (c) iMRE reconstruction of normalized DR (normalized to the mean of DR in the spleen). (d) Extrinsic MR elastography (eMRE) reconstruction at 60 Hz displays increased SS (kPa) in the tumor area. (e) eMRE reconstruction demonstrates a higher DR at 60 Hz in the tumor area. NSS = normalized shear stiffness; NDR = normalized damping ratio; SS = shear stiffness; DR = damping ratio.

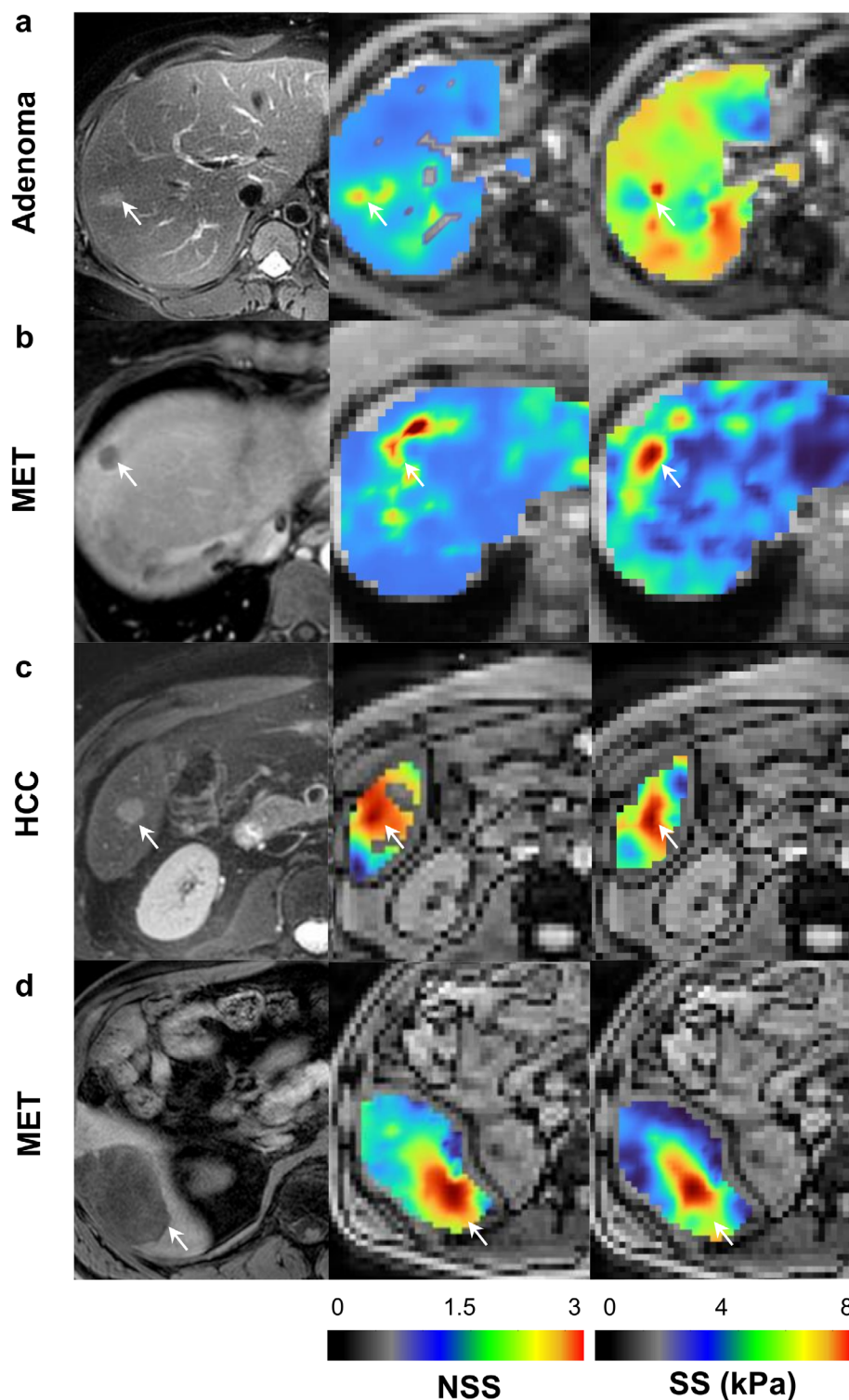


Figure 3: Intrinsic and extrinsic MRE results in four representative cases of benign and malignant liver tumors. Shown are maps of normalized SS and SS (kPa) along with MR images for anatomic orientation. (a) A 35-year-old woman with adenoma, (b) a 42-year-old woman with liver metastasis, (c) a 57-year-old man with a pathology-proven hepatocellular carcinoma (HCC) in the setting of a viral hepatitis B-induced liver cirrhosis, and (d) a 64-year-old man with a pathology-proven liver metastasis from a low-grade intestinal-type adenocarcinoma of the colon, all showed higher normalized SS (iMRE) and SS (eMRE at 60 Hz) than in the background liver tissue. NSS = normalized shear stiffness; SS = shear stiffness.

which correspond to the vessels inside the domain. These vessels create artifacts in the iMRE and have been segmented out from the reconstruction process.

Table 3 summarizes descriptive statistics SS and DR at various frequencies (1, 30, 40, and 60 Hz) for benign and malignant lesions. For each participant, the average value of

Table 3. Viscoelastic Parameters at Different Frequencies for Benign and Malignant Liver Lesions

Lesions	Normalized SS, 1 Hz	Normalized DR, 1 Hz	SS (kPa), 30 Hz	SS (kPa), 40 Hz	SS (kPa), 60 Hz	DR, 30 Hz	DR, 40 Hz	DR, 60 Hz
Benign	Hemangioma	1.01 ± 0.49	0.19 ± 0.49	2.68 ± 0.80	2.16 ± 0.89	2.16 ± 1.67	0.19 ± 0.11	0.26 ± 0.26
	FNH	1.26 ± 0.21	0.15 ± 0.22	2.20 ± 0.89	1.89 ± 0.90	1.89 ± 1.26	0.21 ± 0.05	0.18 ± 0.08
	Hepatocellular adenoma	2.34	0.07	2.35 ± 0.32	2.39 ± 1.22	2.39 ± 0.40	0.22 ± 0.22	0.21 ± 0.05
Malignant	LR-2	-	-	1.94 ± 2.61	2.33 ± 0.80	2.33 ± 0.54	0.37 ± 0.17	0.27 ± 0.07
	LR-3	1.92 ± 1.15	0.17 ± 1.16	3.87 ± 1.71	3.66 ± 1.79	3.66 ± 1.76	0.31 ± 0.10	0.18 ± 0.12
	All benign lesions	1.63 ± 0.45	0.17 ± 0.21	2.60 ± 1.26	2.49 ± 2.74	2.48 ± 1.12	0.21 ± 0.01	0.22 ± 0.09
	LR-4	2.68 ± 0.65	0.05 ± 0.66	4.43 ± 1.60	4.54 ± 1.23	4.53 ± 2.37	0.19 ± 0.88	0.50 ± 0.22
	LR-5	2.39 ± 1.15	0.07 ± 0.16	4.08 ± 1.49	4.86 ± 1.49	4.87 ± 4.43	0.42 ± 0.15	0.66 ± 0.24
	Metastasis	4.54 ± 2.11	0.07 ± 0.11	5.52 ± 1.01	5.67 ± 1.56	8.89 ± 2.18	0.30 ± 0.14	0.73 ± 0.91
	HCC	4.08	0.03	4.85 ± 2.17	6.32 ± 2.30	6.32 ± 2.53	0.51 ± 0.21	2.13 ± 2.01
	Cholangiocarcinoma	4.78	0.68	5.21	8.91	12.01	0.45	0.46
	All malignant lesions	3.69 ± 1.31	0.18 ± 0.23	3.76 ± 1.12	6.06 ± 1.65	7.32 ± 2.87	0.36 ± 0.11	0.89 ± 0.86

Results are presented as mean ± standard deviation.

SS = shear stiffness; DR = damping ratio; FNH = focal nodular hyperplasia; HCC = hepatocellular carcinoma; kPa = kilopascal.

viscoelastic parameters was calculated across all segmented areas, including the liver, lesion, and spleen, segmented by two radiologists (M.B., and E.K.). Normalized SS values for benign and malignant lesions at 1 Hz in iMRE were 1.63 ± 0.45 and 3.69 ± 1.31 , respectively. SS values for benign and malignant lesions at 30 Hz in eMRE were 2.60 ± 1.26 and 3.76 ± 1.12 kPa; at 40 Hz were 2.49 ± 2.74 and 6.06 ± 1.65 kPa; and at 60 Hz were 2.48 ± 1.12 and 7.32 ± 2.87 kPa, respectively. Normalized DR values for benign and malignant lesions at 1 Hz in iMRE were 0.17 ± 0.21 and 0.18 ± 0.23 , respectively. DR values for benign and malignant lesions at 30 Hz were 0.27 ± 0.07 and 0.30 ± 0.11 ; at 40 Hz were 0.21 ± 0.01 and 0.36 ± 0.11 ; and at 60 Hz were 0.22 ± 0.09 and 0.89 ± 0.86 , respectively.

Liver Lesion Classification

Figure 4 shows boxplots of iMRE-determined normalized SS at 1 Hz and extrinsic MRE-determined SS at 30, 40, and 60 Hz for different types of liver lesions, and for benign and malignant liver lesions. There were significant differences in iMRE-determined normalized SS at 1 Hz, and extrinsic MRE-determined SS at 30, 40, and 60 Hz between lesion types. There were significant differences between hemangioma and metastasis, but not between FNH and metastasis ($P = 0.005$) for the intrinsic MRE. There were significant differences between hemangioma and metastasis for 30, 40, and 60 Hz. Furthermore, there were significant differences between FNH and metastasis at 30, 40, and 60 Hz. There were significant differences between benign and malignant lesions in iMRE-determined normalized SS at 1 Hz and eMRE-determined SS at 30, 40, and 60 Hz.

Figure 5 shows boxplots of iMRE-determined normalized DR at 1 Hz and extrinsic MRE-determined DR at 30, 40, and 60 Hz for different types of liver lesions, and for benign and malignant liver lesions. The iMRE-determined normalized DRs were not significantly different between lesion types at 1 Hz ($P = 0.77$) and extrinsic MRE-determined DRs at 30 Hz ($P = 0.06$). However, DRs were significantly different between lesions at 40 and 60 Hz. There were no significant differences between the pairwise groups at any frequency. There were no significant differences in the iMRE-determined normalized DR at 1 Hz ($P = 0.62$). There were no significant differences between benign and malignant lesions in iMRE-determined normalized DR at 1 Hz ($P = 0.62$). There were significant differences between benign and malignant lesions eMRE-determined DR at 30, 40, and 60 Hz.

The interobserver agreement were performed on 15 participants who underwent iMRE. The NLI-iMRE was found to be reproducible, with an ICC of 0.98 (95% CI: 0.92, 1.00) for SS and 0.95 (95% CI: 0.88, 0.97) for the DR. The

Bland–Altman plot is shown in Fig. S2 in the Supplemental Material.

Diagnostic Performance

Table 4 and Figure 6 show the estimates of diagnostic performance and the ROC curves of SS and DR using iMRE at 1 Hz and eMRE at 30, 40, and 60 Hz. These comparisons were made for 32 participants who completed both iMRE and eMRE data acquisition. To differentiate benign and malignant lesions using SS, the AUCs were 0.86 (95% CI: 0.81–0.92) for iMRE at 1 Hz, and 0.87 (0.82–0.89), 0.93 (0.87–0.98), and 0.98 (0.95–1.00) for eMRE at 30, 40, and 60 Hz, respectively. Statistical comparisons of the AUCs between iMRE at 1 Hz and eMRE at all frequencies indicated significant differences. For the DR, the AUCs were 0.47 (0.43–0.55) for iMRE at 1 Hz, and 0.62 (0.58–0.66), 0.81 (0.75–0.87), and 0.86 (0.72–0.95) for eMRE at 30, 40, and 60 Hz, respectively. Parameter SS from eMRE at 60 Hz provided higher AUC than SS at 40 Hz (0.98 vs. 0.93, $P = 0.27$), SS at 30 Hz (0.98 vs. 0.87 $P = 0.44$), and normalized SS at 1 Hz (0.98 vs. 0.86, $P = 0.41$) for distinguishing benign and malignant lesions. Parameter DR from eMRE at 60 Hz provided higher AUC than DR at 40 Hz (0.86 vs. 0.81, $P = 0.21$), DR at 30 Hz (0.86 vs. 0.62, $P = 0.03$), and normalized DR at 1 Hz (0.86 vs. 0.47, significant difference) for distinguishing benign and malignant lesions.

Discussion

This pilot study assessed viscoelastic parameters over a spectrum of focal liver lesions evaluated by iMRE and compared the diagnostic performance of iMRE and eMRE for differentiating benign and malignant nodules. SS, a parameter related to elasticity, was higher in malignant liver lesions compared to benign lesions at all evaluated frequencies, regardless of whether iMRE or eMRE was used. DR, which characterizes the overall viscoelastic behavior of a material, did not show significant differences between malignant and benign lesions at lower frequencies but differed significantly at 40 and 60 Hz with eMRE. The findings demonstrate that eMRE provided superior diagnostic performance at higher frequencies, especially for differentiating lesions based on SS and DR.

The higher stiffness observed in malignant lesions is in agreement with the prior literature.^{6–8} This observation aligns with the established notion that liver tissue undergoes substantial biomechanical changes during malignant transformation, resulting in increased tissue stiffness.² The phenomenon of increased stiffness in malignant lesions is multifactorial, with several underlying elements contributing to this mechanical alteration.²⁵ Indeed, malignancy is associated with a higher mitotic rate, leading to an elevated ratio of nucleus-to-cytoplasm.²⁶ This increased cellular density and nuclear crowding have been associated with greater tissue stiffness.

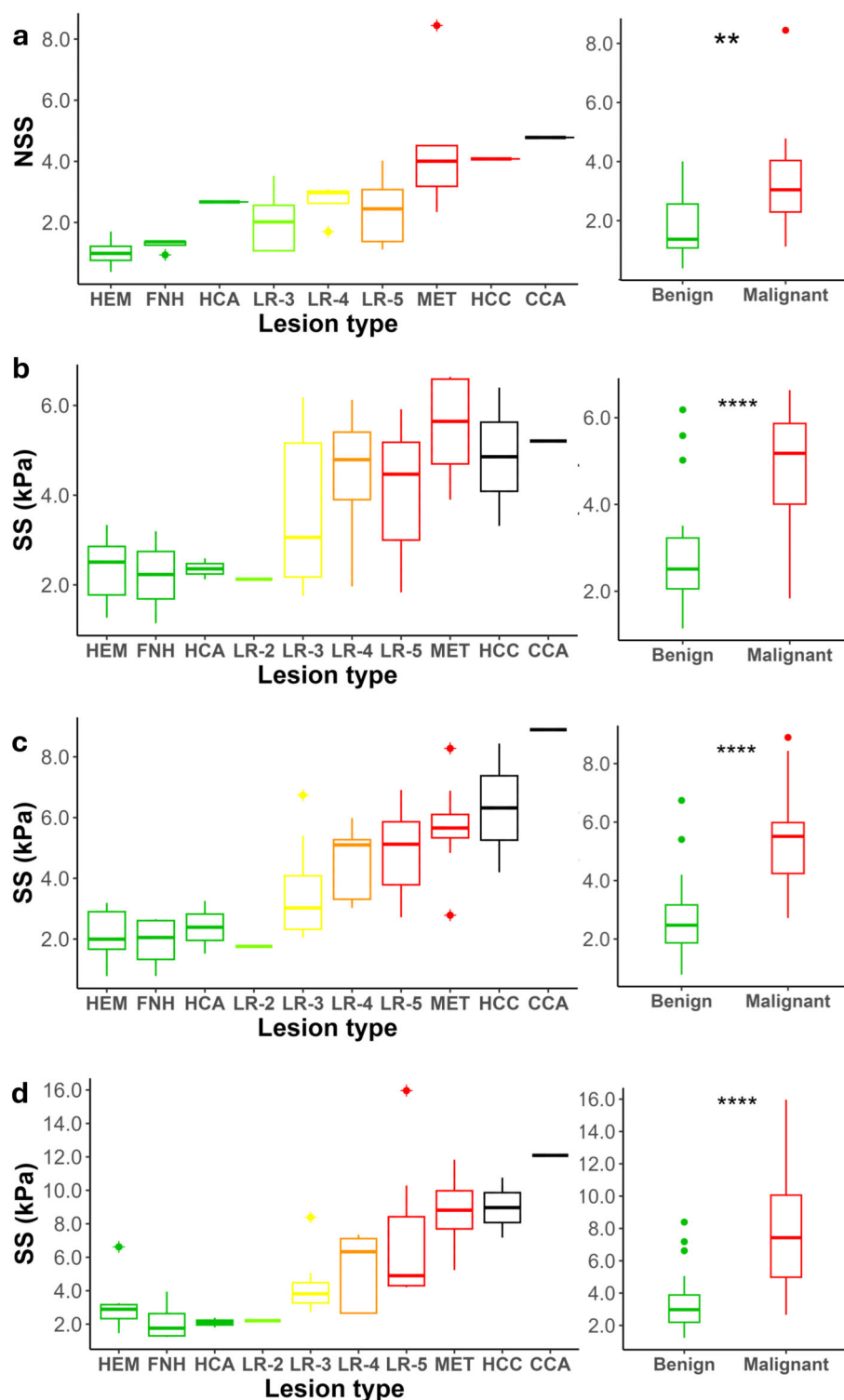


Figure 4: (a) Boxplot of intrinsic MRE-determined normalized SS for different types of liver lesions and for benign and malignant lesions at 1 Hz. (b) Boxplot of extrinsic MRE-determined SS for different types of liver lesions and for benign and malignant lesions at 30 Hz, (c) 40 Hz, and (d) 60 Hz. NSS = normalized shear stiffness; SS = shear stiffness; HEM = hemangioma; FNH = focal nodular hyperplasia; HCA = hepatocellular adenoma; MET = metastasis; HCC = hepatocellular carcinoma; CCA = cholangiocarcinoma.

Furthermore, alterations in the actin cytoskeleton, a crucial component of cellular mechanical properties, play a pivotal role in modulating tissue elasticity. In cancerous tissues,

changes in the actin cytoskeleton can enhance tissue rigidity.²⁷ These findings underscore the potential of iMRE as a tool for assessing these mechanical alterations and providing

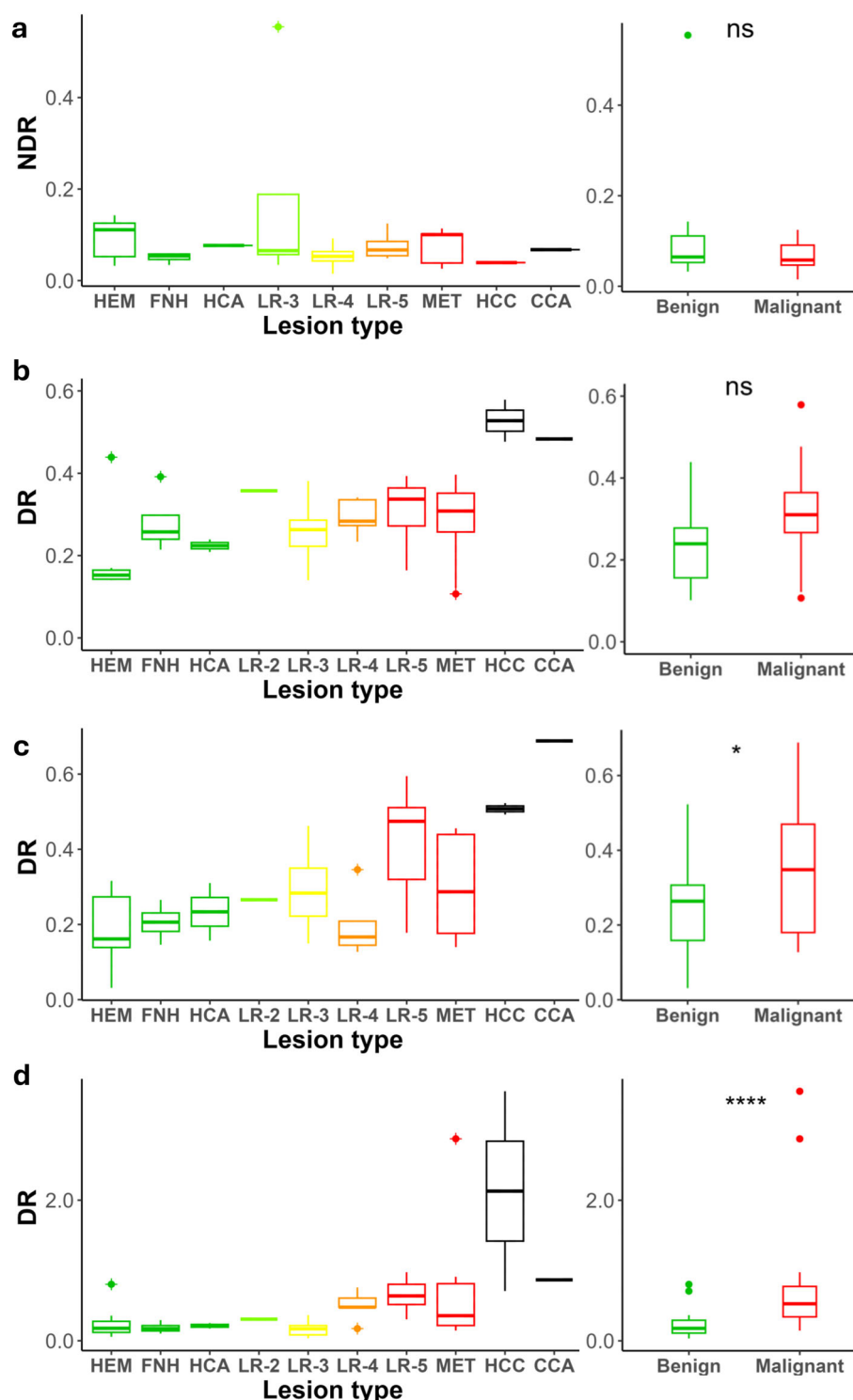


Figure 5: (a) Boxplot of iMRE-determined normalized DR for different types of liver lesions and for benign and malignant lesions at 1 Hz. (b) Boxplot of eMRE-determined DR for different types of liver lesions and for benign and malignant lesions at 30 Hz, (c) 40 Hz, and (d) 60 Hz. NDR = normalized damping ratio; DR = damping ratio; HEM = hemangioma; FNH = focal nodular hyperplasias; HCA = hepatocellular adenoma; MET = metastasis; HCC = hepatocellular carcinoma; CCA = cholangiocarcinoma.

crucial diagnostic information. This has been observed in rabbits with VX2 tumor models that have been performed in vivo elastography of liver cancer.²⁸

In prior human studies, Venkatesh et al reported a greater mean SS in malignant liver lesions (10.1 kPa)

compared to benign lesions (2.7 kPa), based on data from 44 liver lesions using extrinsic MR elastography.⁸ Garteiser et al reported an AUC of 0.77 in 72 lesions using MR elastography with 50-Hz mechanical waves and a full three-directional motion-sensitive sequence, based on the loss

Table 4. Diagnostic Performance of Mechanical Parameters Calculated Using iMRE and eMRE

Technique	Frequency	AUC	Cut-offs	Sensitivity (%)	Specificity (%)	PPV (%)	NPV (%)
iMRE normalized SS	1 Hz	0.86 (0.81–0.92)	≥ 2.72	74 (71–77)	94 (91–95)	92 (89–96)	78 (75–80)
eMRE SS (kPa)	30 Hz	0.87 (0.82–0.89)	≥ 3.15	76 (74–81)	93 (92–97)	85 (82–89)	80 (77–84)
	40 Hz	0.93 (0.87–0.98)	≥ 3.62	94 (89–97)	86 (84–92)	87 (83–91)	93 (91–96)
	60 Hz	0.98 (0.95–1.00)	≥ 4.16	93 (90–95)	100 (95–100)	100 (95–100)	94 (91–95)
iMRE normalized DR	1 Hz	0.47 (0.43–0.55)	≥ 0.13	47 (42–51)	54 (51–61)	52 (48–55)	60 (56–63)
eMRE DR	30 Hz	0.62 (0.58–0.66)	≥ 0.28	54 (50–64)	77 (75–84)	74 (71–77)	74 (71–77)
	40 Hz	0.81 (0.75–0.87)	≥ 0.35	63 (60–66)	87 (85–94)	85 (83–88)	69 (65–73)
	60 Hz	0.86 (0.72–0.95)	≥ 0.36	66 (63–72)	93 (90–95)	95 (90–97)	79 (76–83)

Numbers in parentheses are 95% confidence intervals.

AUC = areas under receiver operating characteristic curves; SS = shear stiffness; DR = damping ratio; PPV = positive predictive value; NPV = negative predictive value.

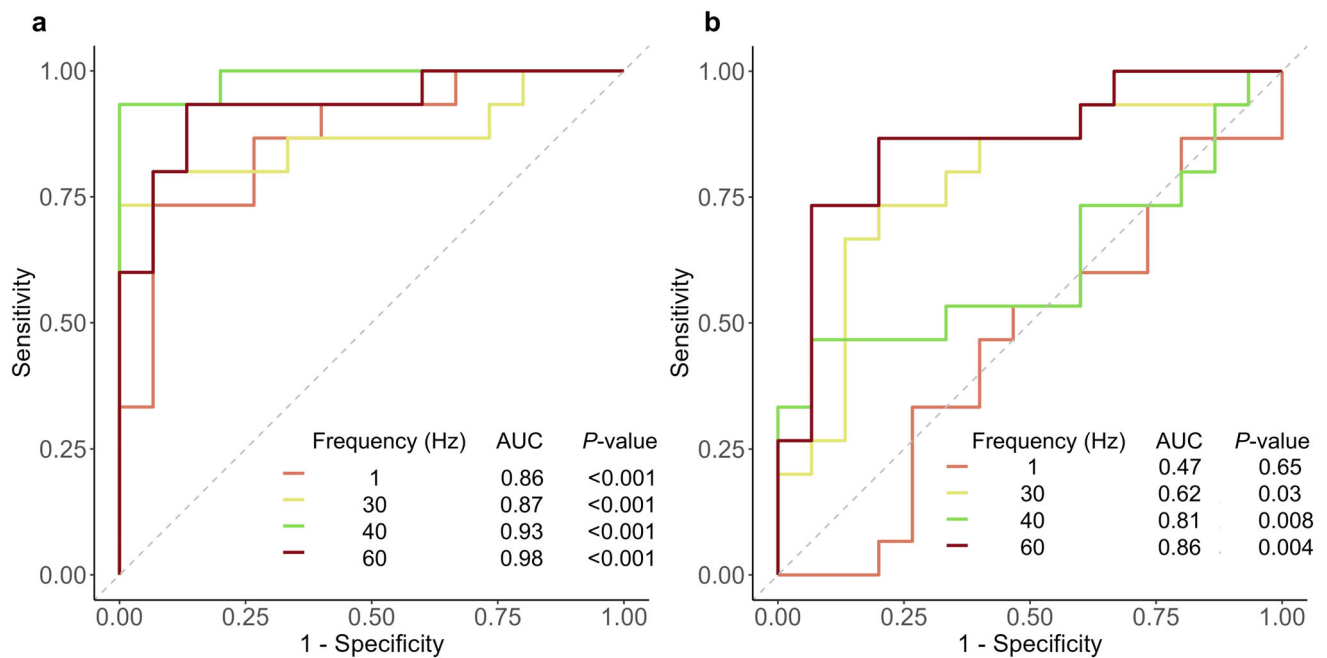


Figure 6: Receiver operating characteristics curve showing (a) SS and (b) DR for classification of benign vs. malignant lesions using intrinsic MRE normalized results at 1 Hz and extrinsic MRE at 30, 40, and 60 Hz.

modulus value, to differentiate between benign and malignant lesions.⁷ Shahryari et al reported an AUC of 0.95 in 77 participants, with a total of 141 focal liver lesions, using the tomoelastography imaging method to compare benign vs. malignant lesions based on the phase angle parameter.⁶ Of

note, all the prior work was performed using ex vivo measurements or in vivo measurements with extrinsic MRE.

This study focused on the normalized DR as an additional parameter for characterizing liver lesions. The results did not reveal a significant difference in the DR across

different lesion types at intrinsic activation frequencies. This finding is consistent with previous observations and highlights the complexity of mechanical properties in liver lesions at these physiological frequencies.¹⁸ The DR for intrinsic data is a parameter that combines the effects of multiple physical phenomena in the tissue, such as poroelastic effects, mechanical wave attenuation due to fluid–solid interaction, and mechanical losses in the tissue. In the extrinsic case at higher frequencies, the first two of these phenomena are relatively small compared to mechanical losses; tissue mostly acts as a viscoelastic material.¹² So, the DR has a clearer physiological correspondence. In the intrinsic case, these different phenomena have similar impacts on the displacement field, making the parameter harder to interpret in terms of a single physiological phenomenon.

Of the two parameters assessed, SS provided the higher AUCs for differentiating benign and malignant liver lesions. Prior studies reporting the *in vivo* mechanical properties of focal liver lesions relied on eMRE.^{6,7} Instead, in this technique, low-frequency, complex-valued harmonic motions at the cardiac pulse frequency were determined via a Fourier transform, and the subzone-based NLI-iMRE reconstruction method was applied to determine the viscoelastic parameters within the imaging volume.

The findings partially align with prior eMRE investigations, such as those by Hennedige et al and Shahryari et al and brain iMRE by Burman et al.^{6,29,30} Notably, the iMRE results, obtained at approximately 1 Hz without the use of external transducers, corroborate Hennedige et al's findings regarding the differentiation of malignant and benign lesions using the storage modulus (G').³⁰ Burman et al's study reveals more consistent results from SS reconstruction than from DR when using intrinsic MRE determined at 7 T.²⁹ Moreover, these results are in agreement with those of Sauer et al who found that changes in tumor stiffness are related to fluid-tissue properties.³¹ This consistency with eMRE findings supports further investigation of iMRE as a noninvasive and hardware-free technique for characterizing liver lesions.

The variation in the results at higher frequencies, particularly at 60 Hz, when compared to the low-frequency intrinsic MRE data, underscores the impact of frequency-dependent mechanical properties in liver tissues.^{32,33} This discrepancy may stem from differences in tissue response to varying frequencies of mechanical wave propagation. Higher frequencies offer advantages such as better resolution of tissue structures, reduced noise interference, and shorter propagation distances within tissues, contributing to the observed differences. This underscores the potential for multifrequency MRE to capture nuanced information about tissue mechanical properties and underscores the importance of choosing an appropriate frequency range for specific diagnostic objectives.³⁴

The characteristic correlation distance in MRE is linked to the mechanical wavelength, which varies with the actuation

frequency. iMRE uses a lower actuation frequency than eMRE, resulting in a higher mechanical wavelength for iMRE. Given the fixed spatial resolution in both iMRE and eMRE, this higher wavelength in iMRE can lead to lower diagnostic performance. Specifically, if the mechanical wavelength is significantly larger than the size of the lesion, the lesion deformation may not be sampled adequately, leading to less precise measurements of mechanical properties. While this study lacked a number of very small lesions with which we could compare the detection limits of iMRE and eMRE for these challenging cases, iMRE was able to detect lesions as small as 15 mm in size. Based on these promising results, future studies of this technique will seek to investigate possible limitations due to lesion size, especially compared to higher-frequency eMRE methods.

The source of vibration in the liver is either from the vasculature or heart movement. Although it has been usually observed that a higher level of strain is on the diaphragmatic side, there are also tumors on the visceral side that can be detected using iMRE. This demonstrates that iMRE is not restricted to a specific area and can effectively measure mechanical properties across the entire liver, regardless of tumor location. demonstrates that iMRE can detect a lesion on the visceral side, where a metastasis case was observed far from the heart.

This study presents potential advantages over the current literature, including the ability to characterize the mechanical properties of liver lesions without using additional hardware. A corollary is the ability to deploy this technique into existing scanners using phase-contrast sequences. In this pilot study, we have demonstrated that iMRE allows the characterization of viscoelastic properties of focal liver lesions. By evaluating tissue stiffness using intrinsic pulsations, iMRE could be added to MRI protocols while providing results similar to that of eMRE.

Limitations

In the intrinsic reconstruction, stiffness values were normalized by their respective values in the spleen. However, mechanical properties of the spleen can undergo alterations due to various factors, such as certain cancers and diseases like portal hypertension, lymphoma, and leukemia.³⁵ Thus, employing the spleen as a reference standard for normalization may present potential challenges. Second, this proof-of-concept study demonstrating the feasibility of iMRE for the characterization of focal liver lesions included only 32 participants. After the initial analysis of the data, the decision to use the spleen as a reference was made retrospectively, resulting in the exclusion of some cases. Future studies should investigate the ability to compute the absolute value of viscoelastic parameters from iMRE without the need for normalization to the spleen. Third, the postprocessing and segmentation time currently does not allow real-time clinical

diagnosis. However, technical improvements and computational power will decrease the postprocessing time. Despite being regarded as benign in the statistical analysis, a recent meta-analysis by Lee et al reported that 31% of LR-3 lesions on MRI performed with extracellular agents are HCC.³⁶ In addition, the study was conducted at a single center using a single vendor, single field strength, and single magnet, which may limit the generalizability of the findings.

Conclusion

This study provides insights into the assessment of liver mechanical properties using iMRE, which does not require an external actuator. We observed higher SS in malignant liver lesions, regardless of whether iMRE or MRE techniques were employed. This finding reinforces the well-established understanding that malignant transformations in liver tissues led to substantial biomechanical changes, resulting in higher tissue SS. This research paves the way for future studies that may refine our understanding of liver biomechanics and contribute to more effective diagnostic and treatment strategies.

Acknowledgments

This research was supported by the Onco-Tech consortium (#293741) composed of the Oncopole, the MEDTEQ Consortium, the TransMedTech Institute, and the Cancer Research Society. An Tang received a Senior salary award from the Fonds de Recherche du Québec en Santé and the Fondation de l'Association des Radiologistes du Québec (FRQS-FARQ 298509).

References

1. Ichikawa S, Motosugi U, Enomoto N, Onishi H. Magnetic resonance elastography can predict development of hepatocellular carcinoma with longitudinally acquired two-point data. *Eur Radiol* 2019;29:1013-1021.
2. Singh S, Fujii LL, Murad MH, et al. Liver stiffness is associated with risk of decompensation, liver cancer, and death in patients with chronic liver diseases: A systematic review and meta-analysis. *Clin Gastroenterol Hepatol* 2013;11(12):1573-1584. e1572.
3. Wang J, Shan Q, Liu Y, et al. 3D MR elastography of hepatocellular carcinomas as a potential biomarker for predicting tumor recurrence. *J Magn Reson Imaging* 2019;49(3):719-730.
4. Jiao Y, Dong F, Wang H, et al. Shear wave elastography imaging for detecting malignant lesions of the liver: A systematic review and pooled meta-analysis. *Med Ultrason* 2017;19(1):16-22.
5. Van Houten EE, Doyle MM, Kennedy FE, Paulsen KD, Weaver JB. A three-parameter mechanical property reconstruction method for MR-based elastic property imaging. *IEEE Trans Med Imaging* 2005;24(3):311-324.
6. Shahyari M, Tzschätzsch H, Guo J, et al. Tomoelastography distinguishes noninvasively between benign and malignant liver lesions. *Cancer Res* 2019;79(22):5704-5710.
7. Garteiser P, Doblas S, Daire J-L, et al. MR elastography of liver tumours: Value of viscoelastic properties for tumour characterisation. *Eur Radiol* 2012;22:2169-2177.
8. Venkatesh SK, Yin M, Glockner JF, et al. Magnetic resonance elastography of liver tumors-preliminary results. *AJR Am J Roentgenol* 2008;190(6):1534-1540.
9. Weaver JB, Pattison AJ, McGarry MD, et al. Brain mechanical property measurement using MRE with intrinsic activation. *Phys Med Biol* 2012;57(22):7275-7287.
10. Lefebvre T, Petitclerc L, Hébert M, et al. MRI cine-tagging of cardiac-induced motion for noninvasive staging of liver fibrosis. *J Magn Reson Imaging* 2020;51(5):1570-1580.
11. Van Houten E, Gilbert G, Tang A. Actuator-free MR elastography of the liver: Imaging liver tumors with viscoelastic intrinsic MRE. In: *ISMRM & SMRT Virtual Conference & Exhibition*. 2020.
12. McGarry M, Van Houten E, Solamen L, Gordon-Wylie S, Weaver J, Paulsen K. Uniqueness of poroelastic and viscoelastic nonlinear inversion MR elastography at low frequencies. *Phys Med Biol* 2019;64(7):075006.
13. Kennedy P, Wagner M, Castéra L, et al. Quantitative elastography methods in liver disease: Current evidence and future directions. *Radiology* 2018;286(3):738-763.
14. Yin M, Glaser KJ, Manduca A, et al. Distinguishing between hepatic inflammation and fibrosis with MR elastography. *Radiology* 2017;284(3):694-705.
15. Allen AM, Shah VH, Therneau TM, et al. The role of three-dimensional magnetic resonance elastography in the diagnosis of nonalcoholic steatohepatitis in obese patients undergoing bariatric surgery. *Hepatology* 2020;71:510-521.
16. Yin Z, Murphy MC, Li J, et al. Prediction of nonalcoholic fatty liver disease (NAFLD) activity score (NAS) with multiparametric hepatic magnetic resonance imaging and elastography. *Eur Radiol* 2019;29:5823-5831.
17. Komiya Y, Motosugi U, Maekawa S, et al. Early diagnosis of hepatic inflammation in Japanese nonalcoholic fatty liver disease patients using 3D MR elastography. *Hepatol Res* 2023;53(3):208-218.
18. Gordon-Wylie SW, Solamen LM, McGarry MD, et al. MR elastography at 1 Hz of gelatin phantoms using 3D or 4D acquisition. *J Magn Reson* 2018;296:112-120.
19. Garteiser P, Sahebjavaher RS, Ter Beek LC, et al. Rapid acquisition of multifrequency, multislice and multidirectional MR elastography data with a fractionally encoded gradient echo sequence. *NMR Biomed* 2013;26(10):1326-1335.
20. Van Houten EE, Paulsen KD, Miga MI, Kennedy FE, Weaver JB. An overlapping subzone technique for MR-based elastic property reconstruction. *Magn Reson Med* 1999;42(4):779-786.
21. Hiscox LV, McGarry MD, Schwarb H, et al. Standard-space atlas of the viscoelastic properties of the human brain. *Hum Brain Mapp* 2020;41(18):5282-5300.
22. Fedorov A, Beichel R, Kalpathy-Cramer J, et al. 3D Slicer as an image computing platform for the quantitative imaging network. *Magn Reson Imaging* 2012;30(9):1323-1341.
23. Cunha GM, Fowler KJ, Roudenko A, et al. How to use LI-RADS to report liver CT and MRI observations. *Radiographics* 2021;41(5):1352-1367.
24. DeLong ER, DeLong DM, Clarke-Pearson DL. Comparing the areas under two or more correlated receiver operating characteristic curves: A nonparametric approach. *Biometrics* 1988;44:837-845.
25. Koumoutsakos P, Pivkin I, Milde F. The fluid mechanics of cancer and its therapy. *Annu Rev Fluid Mech* 2013;45:325-355.
26. Nagar V, Ye J, Ng W, et al. Diffusion-weighted MR imaging: Diagnosing atypical or malignant meningiomas and detecting tumor dedifferentiation. *Am J Neuroradiol* 2008;29(6):1147-1152.
27. Wells RG. The role of matrix stiffness in regulating cell behavior. *Hepatology* 2008;47(4):1394-1400.
28. Zhao X, Zheng Y, Liang J, et al. In vivo tumor detection on rabbit with biopsy needle as MRE driver. In: *2008 30th Annual International Conference of the IEEE Engineering in Medicine and Biology Society: IEEE*; 2008. p 121-124.

29. Burman IM, Van Houten E, Zwanenburg JJ. Estimating the viscoelastic properties of the human brain at 7 T MRI using intrinsic MRE and nonlinear inversion. *Hum Brain Mapp* 2023;44:6575-6591.
30. Hennedige TP, Hallinan JTPD, Leung FP, et al. Comparison of magnetic resonance elastography and diffusion-weighted imaging for differentiating benign and malignant liver lesions. *Eur Radiol* 2016;26:398-406.
31. Sauer F, Grosser S, Shahyari M, et al. Changes in tissue fluidity predict tumor aggressiveness in vivo. *Adv Sci* 2023;10(26):2303523.
32. Asbach P, Klatt D, Hamhaber U, et al. Assessment of liver viscoelasticity using multifrequency MR elastography. *Magn Reson Med* 2008;60(2):373-379.
33. Tzschätzsch H, Ipek-Ugay S, Guo J, et al. In vivo time-harmonic multifrequency elastography of the human liver. *Phys Med Biol* 2014;59(7):1641-1654.
34. Mariappan YK, Glaser KJ, Ehman RL. Magnetic resonance elastography: A review. *Clin Anat* 2010;23(5):497-511.
35. Garteiser P, Doblas S, Van Beers BE. Magnetic resonance elastography of liver and spleen: Methods and applications. *NMR Biomed* 2018;31(10):e3891.
36. Lee S, Kim Y-Y, Shin J, et al. Percentages of hepatocellular carcinoma in LI-RADS categories with CT and MRI: A systematic review and meta-analysis. *Radiology* 2023;307(1):e220646.